

RSC Advances



This is an *Accepted Manuscript*, which has been through the Royal Society of Chemistry peer review process and has been accepted for publication.

Accepted Manuscripts are published online shortly after acceptance, before technical editing, formatting and proof reading. Using this free service, authors can make their results available to the community, in citable form, before we publish the edited article. This *Accepted Manuscript* will be replaced by the edited, formatted and paginated article as soon as this is available.

You can find more information about *Accepted Manuscripts* in the [Information for Authors](#).

Please note that technical editing may introduce minor changes to the text and/or graphics, which may alter content. The journal's standard [Terms & Conditions](#) and the [Ethical guidelines](#) still apply. In no event shall the Royal Society of Chemistry be held responsible for any errors or omissions in this *Accepted Manuscript* or any consequences arising from the use of any information it contains.



Solvent- and catalyst-free synthesis of fully biobased nonisocyanate polyurethanes with different macromolecular architectures.

Received 00th January 20xx,
Accepted 00th January 20xx

DOI: 10.1039/x0xx00000x

www.rsc.org/

C. Carré,^a L. Bonnet^a and L. Avérous^a

A bis(cyclic carbonate) based on a dimeric fatty acid was successfully synthesized. The chemical structure of the original cyclic carbonate and its intermediates were determined by FTIR and NMR analyses. The cyclic carbonate reacted with a dimer-based diamine to give a fully biobased nonisocyanate polyurethane (NIPU), without solvent and catalyst. Different macromolecular architectures were obtained. The influence of the cyclic carbonate:amine ratio, and the effect of the average amine functionality were investigated by chemical, thermal and rheological analyses, respectively. These parameters strongly impact the final NIPU properties. Comparison with NIPUs based on linear structures show the effect of the architecture introduced by the dimer-based building blocks on the resulting NIPU properties. To evaluate the real potential of these novel materials, NIPUs were also compared to conventional polyurethanes with equivalent architectures.

1. Introduction

Currently, literature shows more and more scientific papers about biobased PUs. In most cases only the polyols are biobased, since the isocyanates remain fossil-based.¹⁻⁴ However, to increase the renewable carbon content, some scientists have developed vegetable oil-based isocyanates,⁵⁻⁸ to produce fully biobased PUs.⁹ Although several very promising molecules have been developed, a simple substitution with biobased products cannot solve the arising problems linked to the use of harmful and potentially carcinogenic isocyanates. Repetitive exposure to them can lead to serious and incurable respiratory problems.¹⁰ Moreover, the synthesis of isocyanates requires the use of noxious substances such as phosgene.

The current trend, linked to the evolution of national and international regulations, is thus to move from petrochemical PUs to promising biobased ones, without isocyanates.² To answer to environmental and health concerns, a new range of polyurethanes called Nonisocyanate PolyUrethanes (NIPUs) is now emerging. One of the main ways to obtain NIPUs is by aminolysis synthesis. Through an amine-cyclocarbonate reaction, NIPUs can be prepared without the use of toxic isocyanate.^{2, 11, 12} These NIPUs are also called polyhydroxyurethanes (PHUs), since they contain some hydroxyl groups due to the cyclic carbonate ring opening.¹³

Cyclic dicarbonates can be synthesized by various methods,¹⁴ such as the direct esterification of dicarboxylic acids with glycerol carbonate, a promising route using renewable resources. Glycerol carbonate, a cheap and widely available biobased building block, is obtained from the reaction of carbon dioxide and glycerol, a major by-product from the oleochemistry and biodiesel industries, for example.¹⁵ Diamines and their corresponding dicarboxylic acids can be produced from biobased feedstocks, and more particularly from vegetable oils. In addition to linear fatty diacids obtained from oxidative cleavage (ozonolysis, alkali fusion, etc.),^{16, 17} methoxycarbonylation,¹⁸ metathesis¹⁹ or microbial oxidation,²⁰ dimeric fatty acids (DFAs) can also be produced by dimerization of unsaturated fatty acids (Diels-Alder reaction) derived from vegetable oils such as rapeseed or soybean oils. An example of the corresponding chemical structures is given in Figure 1. In addition to diacids, and due to specific processing conditions (200-250°C under pressure in the presence of catalysts), monoacids and triacids can also result from this reaction. Distillation and hydrogenation steps can then be performed depending on the desired purity and final structures. Dimeric diamines (DDAs) can result from the synthesis of DFAs with ammonia followed by a reduction reaction.²¹ DFAs and DDAs are promising biobased (100% renewable carbon content) building blocks for the preparation of new durable, biobased macromolecular architectures. Thanks to their unique structures with long pendant chains, they provide the resultant polymers with specific properties such as high flexibility and low glass transition temperatures. Furthermore, they show a low viscosity, which is required for solvent-free synthesis.

^a BioTeam/ICPEES-ECPM, UMR 7515, Université de Strasbourg, 25 rue Bequerel, 67087 Strasbourg Cedex 2, France.

Electronic Supplementary Information (ESI) available: [details of any supplementary information available should be included here]. See DOI: 10.1039/x0xx00000x

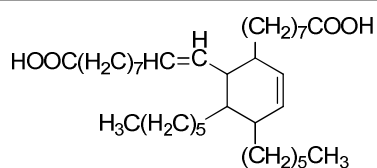


Figure 1. Cyclic chemical structure of a dimeric fatty acid.

In the literature, several papers have highlighted the influence of the chemical structures of cyclic carbonate and diamine on their respective reactivity for NIPU synthesis.²²⁻²⁶ The key factors relating to the reactivity of the cyclic carbonate are the presence and nature of substituents, as well as the number of atoms in the cyclic carbonate ring.^{13, 23, 27} It has already been demonstrated that cyclic carbonates with larger ring sizes present the highest reactivity towards amines, with an increase of the reaction rate²² and the resulting molar mass.²³ Although, it seems that the corresponding cyclic carbonates are responsible for more secondary reactions.²⁸ Furthermore, reactivity is also enhanced when the substituent of the cyclic carbonate is a stronger electron-withdrawing group.²⁷ Concerning diamines, the highest cyclic carbonate reactivity was observed for lower mass aliphatic amines.²⁴ The type of diamine also plays a key role in the aminolysis reaction, since primary amines are reactive towards cyclic carbonates, whereas tertiary amines do not react. Recently, it was shown that secondary amines can also react with carbonates under certain conditions.²⁵ Furthermore, less hindered and more nucleophilic amines display the highest reactivity.²⁶ Contrary to the effect of the structure on the reactivity reported by several groups,^{24, 25, 27} the influence of monomer structure on NIPU properties has not yet been studied.

The aim of this study is to synthesize novel and fully biobased NIPUs *via* a green chemistry process, without solvents and catalysts. We have, therefore, focused our investigations on the use of DFAs and DDAs from vegetable oils. Furthermore, comparisons with NIPUs containing linear structures were carried out to show the influence of the specific dimeric architectures on the resulting NIPU properties. In order to evaluate the real potential of these novel isocyanate-free PUs, comparisons with conventional PUs based on similar macromolecular architectures were also performed. To the best of our knowledge PU synthesis has never been reported from two different dimeric fatty acid derivatives, polyols and polyisocyanates, respectively.

2. Experimental part

2.1. Materials

Radiacid 0970, a dimeric fatty acid (DFA), was provided by Oleon (Ertvelde, Belgium). Table 1 shows its wt.% composition of monomers, dimers and trimers. Figure 1 is one possible orientation for this DFA but noncyclic, mono and bicyclic structures also exist. Thionyl chloride ($\geq 99\%$), ethyl acetate ($\geq 99\%$) and dichloromethane (DCM, $\geq 99\%$) were purchased from Sigma-Aldrich. Glycerol carbonate (Jeffsol GC, 93%) was obtained from Huntsman

(Everberg, Belgium). A dimer-based diol (DOH) and dimer-based diamines (DDAs) were kindly supplied by Croda (Goole, England), under the trade name Pripol 2033 and Priamine, respectively. Two grades of DDA, hereinafter referred to as DDA2.2 and DDA2.0, were used neat or mixed together to obtain a precise average amine functionality. DDA2.2 and DDA2.0 have an average functionality of 2.2 and 2.0, respectively. Dimer and trimer contents are reported in Table 1. The latter present an amine value (AV) of 198 and 204 mg KOH per g, respectively, with glass transition temperatures lower than -50°C . At room temperature, DDA2.2 is a viscous amber liquid, and DDA2.0 is a yellowish, slightly viscous liquid. Diaminooctane (DA8, $>98\%$) and sebacyl chloride (SBCl, 97%) were purchased from Alfa Aesar, and triethylamine from Carlo Erba, respectively. 2-heptyl-3,4-bis(9-isocyanatononyl)-1-pentylcyclohexane, commercialized under the trade name DDI 1410 ($>98\%$), was kindly supplied by Cognis-BASF. Hexamethylene diisocyanate (HDI, $>99.5\%$) was provided by Vencorex (Waalwijk, Netherlands). All chemicals were used as received without any purification with the exception of DCM, which was purified with on a solvent drying station. Table 1 presents an overview of the compositions of the different dimeric materials.

Table 1. Summary of the dimeric materials used and their corresponding contents.

Samples	Monomer content (wt%)	Dimer content (wt%)	Trimer content (wt%)
Radiacid 0970 (DFA)	0.7	96.7	2.6
Priamine 1071 (DDA2.2)	trace amount	75	25
Priamine 1075 (DDA2.0)	trace amount	>99	<1
Pripol 2033 (DOH)	0.5	98.6	0.9
DDI 1410	trace amount	≥ 98	<2

Data obtained from suppliers.

2.2. Synthesis

Two types of BisCC, referred to as SBBisCC and DBisCC, were synthesized. They display linear and dimeric structures, respectively.

Sebacyl bis(cyclo)carbonate (SBBisCC) was directly synthesized by esterification of sebacyl chloride using glycerol carbonate (GC) according to a previously reported procedure.²⁹

Dimeric bis(cyclo)carbonate (DBisCC) was obtained by esterification of a dimeric fatty acid (DFA) with GC. In order to improve the reactivity of DFA, a preliminary halogenation reaction of the compound was carried out. DBisCC was, thus, synthesized in two steps following the general pathway given in Figure 2.

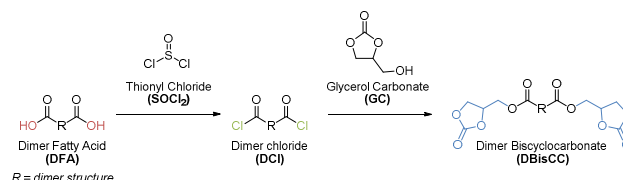


Figure 2. Reaction scheme for the synthesis of DBisCC.

Halogenation step. In a three-necked 250 mL round-bottomed flask equipped with a magnetic stirrer, DFA (20.0 g, 35 mmol) was dissolved into ethyl acetate (100 mL) under a nitrogen flow at a temperature of 35°C. An excess of thionyl chloride (16.7 g, 140 mmol) was then added dropwise through the stirred reaction mixture, which was continuously heated at 35°C over 4 hours. The hydrogen chloride produced was trapped in a wash-bottle containing an aqueous solution of sodium hydroxide connected to the reaction flask *via* an outlet. The solvent and the excess of thionyl chloride were then distilled out from the reaction mixture. Dimer chloride (DCI) was obtained in a yield of 21.3 g (100%), as a brown viscous product. The halogenation reaction was confirmed by IR and NMR analyses.

Esterification step. The esterification step was carried out in a three-necked 250 mL round-bottomed flask. Glycerol carbonate (15.5 g, 131.3 mmol) and triethylamine (13.3 g, 131.4 mmol) were successively introduced into the flask and mixed under an inert gas flow with 50 mL of freshly dried dichloromethane. DCI (20 g, 32.8 mmol) was then added dropwise to the stirred reaction mixture, while cooling in an ice water bath. The reaction was then allowed to proceed overnight at room temperature under agitation under a continuous nitrogen stream. The formed triethylamine hydrochloride $\text{Et}_3\text{N}\cdot\text{HCl}$ was then removed by filtration and the organic phase was washed with a 5 wt.% HCl solution and water to eliminate the excess of glycerol carbonate. The solution was finally dried with anhydrous sodium sulphate and the solvent was removed under vacuum to yield 25.2 g (99.5%) of DBisCC, a brown viscous liquid.

Two classes of NIPU, referred to as linear aliphatic NIPUs (LNIPUs) and dimer-based NIPUs (DNIPUs), were synthesized. They were obtained from linear SBBisCC and dimeric DBisCC, respectively. The formulations of all NIPU samples are summarized in Table 2, with their corresponding designations. LNIPUs were prepared in bulk and without catalyst at 75°C. SBBisCC and various diamines were added at a molar stoichiometric ratio, according to a methodology already reported.²⁹ DNIPUs were obtained *via* the aminolysis reaction between a BisCC and a diamine. A general synthesis was carried out as follows (Monomer ratios are given in Table 2); in a 100 mL reactor equipped with a mechanical stirrer, DBisCC (20.0 g, 25.9 mmol) and diamine were added at a molar stoichiometric ratio. The reaction took place in bulk and without catalyst under inert gas flow at a temperature of 75°C. After two hours with constant stirring, the viscous mixture was spread on a polytetrafluoroethylene-based sheet and heated in an oven under vacuum at 75°C for ninety-four hours. The product was obtained as a yellow or brown solid depending on the diamine used.

Two classes of PU, referred to as LPUs and DPUs, were synthesized. They were respectively obtained from linear (HDI) or dimeric (DDI 1410) isocyanate and two types of polyols following the ensuing general protocol. The formulations of all PU samples are summarized in Table 3.

Table 2. Formulations for the synthesis of the different NIPU samples and their corresponding designations.

Sample	NIPU family	BisCC	Diamine	Corresponding quantities for NIPU synthesis ^a				
				BisCC	Diamine			
					DDA2.0	DDA2.2		
LNIPU-DA8			DA8	7.2 (49.7)	-			
LNIPU-DDA2.0			DDA2.0	27.3 (49.7)	-			
LNIPU-DDA2.05	LNIPU	SBBisCC	DDA2.05	20.0 (49.7)	20.5 (37.3)	7.7 (12.4)		
LNIPU-DDA2.1			DDA2.1				13.7 (24.9)	15.5 (24.9)
LNIPU-DDA2.15			DDA2.15				6.8 (12.4)	23.2 (37.3)
LNIPU-DDA2.2			DDA2.2				-	31.0 (49.7)
DNIPU-DA8			DA8	3.7 (25.9)	-			
DNIPU-DDA2.0			DDA2.0	14.2 (25.9)	-			
DNIPU-DDA2.05	DNIPU	DBisCC	DDA2.05	20.0 (25.9)	10.7 (19.4)	4.1 (6.5)		
DNIPU-DDA2.1			DDA2.1				7.1 (13.0)	8.1 (13.0)
DNIPU-DDA2.15			DDA2.15				3.6 (6.5)	12.1 (19.4)
DNIPU-DDA2.2			DDA2.2				-	16.1 (25.9)

^aInitial formulations for the synthesis of the different NIPUs in g. The molar masses (in mmol) are given in parentheses.

The typical procedure for the synthesis of Pus was carried out as follows. Isocyanate and polyol (see Table 3 for corresponding quantities) were charged in a 100 mL reactor equipped with a mechanical stirrer. The NCO:OH molar ratio was calculated on the basis of the hydroxyl index (I_{OH}) of the polyol and the NCO content (NCO%) of the isocyanate, which were previously determined (Titration methods given in the ESI†). A molar ratio equal to 1.05 was used for all the syntheses. This 5 mol% excess of isocyanate was used to compensate for possible side reactions due to the estimated residual water present in the dried polyols. The main reaction took place in bulk without catalyst at a temperature of 75°C under a dry nitrogen gas flow to prevent the reaction of the isocyanate groups with air moisture. After two hours of continuous stirring, the viscous mixture was spread on a polytetrafluoroethylene-based sheet and heated in an oven under vacuum at 75°C for ninety-four hours. The product was obtained as a yellow or colorless solid depending on the raw materials used.

Table 3. Formulations of the different conventional PU samples and their corresponding designations.

Sample	PU Family	isocyanate	polyol	PU formulation ^a	
				isocyanate	polyol
LPU-DOH	LPU	HDI	DOH	5.1 (60.3)	15 (57.4)
DPU-OH8	DPU	DDI 1410	OH8	20.0 (61.1)	4.3 (58.2)
DPU-DOH			DOH	20.0 (61.1)	15.2 (58.2)

^aInitial composition (in g) of the different synthesized NIPUs. The molar masses (in mmol) are given in parentheses.

2.3. Measurements

Infrared spectroscopy was performed with a Nicolet 380 Fourier transform infrared spectrometer (*Thermo Electron Corporation*) used in Reflection Mode and equipped with an ATR diamond module (FTIR-ATR). The FTIR-ATR spectra were collected at a resolution of 4 cm⁻¹ with 64 scans per run.

¹H- and ¹³C-NMR spectra were recorded on a *Bruker Ascend™* 400 spectrometer at 300 MHz and 100 MHz respectively. Chloroform-d₆ was used as a solvent.

DOSY NMR spectra were recorded on a *Bruker Avance* 400 MHz spectrometer using a QNP 5 mm gradient probe. The temperature was regulated at 300 K and the NMR tube was not spun. The diffusion NMR experiments were performed with a pulsed-gradient stimulated echo sequence using a bipolar gradient.³¹ The samples were prepared by dissolution in deuterated water (D₂O) at a concentration of approx. 10 mg.ml⁻¹. Sequence delays were Δ = 150 ms (diffusion delay), τ = 0.4 ms (after gradient recovery delay), and Te = 2.6 ms (LED recovery delay). Additional information is available in the ESI†.

Thermal degradations were studied by thermogravimetric analyses (TGA). Measurements were conducted under inert gas (flow rate = 25 mL.min⁻¹) using a Hi-Res TGA Q5000 apparatus from *TA Instruments*. The samples (3–5 mg in an aluminum pan) were heated to 600°C at 10°C.min⁻¹. The characteristic degradation temperatures are the those at the maximum of the derivative

thermogram (DTG) curve (T_{max}), and also those at 98%, 50% and 2% of the initial weight (T_{98%}, T_{50%} and T_{2%}).

The main characteristic temperatures were determined by differential scanning calorimetry (DSC Q200, *TA Instruments*), under nitrogen flow. The samples (2–5 mg) were heated to 175°C with a heating rate of 10°C.min⁻¹ (first heating scan), then cooled to -80°C at 5°C.min⁻¹ and finally re-heated to 175°C at a heating rate of 10°C.min⁻¹ (second heating scan). The glass transition temperature (T_g) was determined as the midpoint of the change in slope of the baseline from the second heating scan in order to erase the previous thermal history of the samples during the first scan.

The number-average molar mass (M_n), the mass-average molar mass (M_w) and the dispersity (Đ) of the resulting samples were determined by size exclusion chromatography (SEC) using a Malvern Instrument apparatus (*Viscotek RImax*). This device was equipped with a 10 mm guard column (8 μm) and three 300 mm columns (50, 150 and 500 Å). Refractive index (RI) and ultraviolet (UV) detectors were used. Tetrahydrofuran (THF) was used as the eluent at a flow rate of 1 mL.min⁻¹. The apparatus was calibrated with linear polystyrene standards from 162 to 20,000 g.mol⁻¹.

Degree of swelling (SR) were calculated using Eq. 1, where W_s is the weight of the solvent at equilibrium and W_D is the weight of dry polymer after swelling.

$$SR (\%) = \frac{W_s - W_D}{W_D} \cdot 100 \quad (1)$$

The gel content was determined for each system from Eq. 2, where, W_{p0} is the initial sample weight.

$$G = \frac{W_p}{W_{p0}} \cdot 100 \quad (2)$$

Dynamic rheological analyses (DRA) of the final materials were performed with a strain-controlled rheometer (ARES, Rheometric Scientific) equipped with parallel-plate geometries. The oscillatory measurements were carried out on a 25 mm diameter plate with 2 mm thickness. The following tests were conducted: (i) dynamic strain sweep to estimate the viscoelastic region of the samples, (ii) isofrequency dynamic temperature sweep from 0 to 160°C at a frequency of 1 Hz. Changes in the viscous and storage modulus (G'' and G', respectively) were registered and the corresponding tan δ = G''/G' determined.

Uniaxial tensile tests were performed using an Instron machine (type 5567, H1592 series). The experiments were performed on tensile specimens (size: 25 x 4 x 1 mm) at room temperature using a crosshead speed of 100 mm.min⁻¹ and a load cell of 5 kN sensitivity. After optimising the parameters, experiments were carried out at least 3 times for each sample. Young's modulus (E), tensile strength at break (σ_{max}) and elongation at break (ε_{max}) were determined.

3. Results and discussion

The results are presented in five sections. Firstly, the characterization of the DFA raw material is outlined to clearly define its chemical structure. Afterwards, the characterization of the intermediate products DCI and DBisCC is presented to confirm the chemical modifications of the DFA. The properties of DNIPUs are then explained and compared with NIPU materials based on

more classical linear structures. The last part is dedicated to the comparison of the obtained NIPUs with conventional PUs.

3.1. Chemical characterizations of DFA, DCI and DBISCC

The main chemical characteristics of DFA DCI and DBISCC were reported in Table 4. Main FTIR and $^1\text{H-NMR}$ results are presented in Figures 3 and 4.

The chemical structure of DFA were analyzed by FTIR and NMR spectroscopies (Figure S1 in the ESI⁺ gives $^{13}\text{C-NMR}$ analysis) and gave the following results:

FTIR-ATR (cm^{-1} , Figure 3): 1707 (C=O carbonyl group).

$^1\text{H-NMR}$ (400 MHz, CDCl_3 , δ , ppm Figure 4): 0.85-0.93 (6H, m, -CH₃), 1.26 (38H, s, -CH₂-), 1.58-1.68 (4H, m, -CH₂-CH₂-COOH), 2.35 (4H, t, $J = 7.4$ Hz, -CH₂-COOH), 5.01-5.46, 6.69-7.08 (0.31H, m, -CH=CH-), 11.36 (2H, s, -COOH-).

$^{13}\text{C-NMR}$ (100 MHz, CDCl_3 , δ , ppm Figure S4 in the ESI⁺): 14.3 (-CH₃), 22.8 (-CH₂-CH₃), 24.9 (-CH₂-CH₂-COOH), 29.2-30.3 (-CH₂-), 34.3 (-CH₂-COOH), 180.7 (-COCl).

After dimerization and purification, partial hydrogenation was performed to reduce the double bond content and improve the long-term stability and ageing of this building block. The number of residual double bonds was quantified by $^1\text{H-NMR}$ analysis. Table 4 and the corresponding analysis previously presented shows that DFA has a low number of double bonds per molecule, which is equal to 0.15 per molecule on average. SEC analysis results are higher than expected. This is likely due to the fact that determination of molar masses by SEC is based on a calibration with equivalent PS molar masses, and as such, not perfectly adapted for the analysis of such molecules. Nevertheless, the SEC chromatogram of DFA (Figure S2 in the ESI⁺) displays a well defined double peak, which corresponds to dimer and trimer molecules, with a higher content of dimer structures. All these results are in good agreement with the data given by the supplier.

Diffusion ordered spectroscopy, also called DOSY NMR spectroscopy, was performed to deeply analyze the chemical structure of the DFA raw material without any preliminary physical separation (Figure S3 in the ESI⁺).³¹ All spots of the DFA samples are perfectly aligned suggesting a unique D coefficient. The product presents a low dispersity. From these data, we can confirm the cyclic content value, on agreement with data from the supplier (75% linear, 25% cyclic).

Table 4. Results of analyses performed on the DFA raw product.

SEC analysis	Peak #1	Peak #2
M_n (g.mol^{-1})	808	M_n (g.mol^{-1}) 1304
M_w (g.mol^{-1})	827	M_w (g.mol^{-1}) 1331
$\text{D} (=M_w/M_n)$	1.02	$\text{D} (=M_w/M_n)$ 1.02
% area	93	% area 7
$^1\text{H-NMR}$ analysis	Nber of double bonds per molecule 0.15	
DOSY NMR analysis	Dispersity low	
Titration	Acid value (mg KOH/g) 219.8	

Halogenation of DFA with thionyl chloride yields DCI. The chemical structure of DCI were analyzed and confirmed by FTIR and NMR spectroscopies (Figures 3, 4 and S4 in the ESI⁺) gave the following results:

FTIR-ATR (cm^{-1} , Figure 3): 1798 (C=O chloride group).

$^1\text{H-NMR}$ (400 MHz, CDCl_3 , δ , ppm, Figure 4): 0.85-0.90 (6H, m, -CH₃), 1.26 (38H, s, -CH₂-), 1.65-1.76 (4H, m, -CH₂-CH₂-COCl), 2.88 (4H, t, $J = 7.4$ Hz, -CH₂-COCl), 4.97-5.44, 6.69-7.12 (0.93H, m, -CH=CH-).

$^{13}\text{C-NMR}$ (100 MHz, CDCl_3 , δ , ppm, Figure S4 in the ESI⁺): 14.3 (-CH₃), 22.8 (-CH₂-CH₃), 25.2 (-CH₂-CH₂-COCl), 28.6-29.9 (-CH₂-), 47.3 (-CH₂-COCl), 174.0 (-COCl).

The FTIR spectrum of DFA displayed an absorption band at 1707 cm^{-1} , assigned to the carbonyl group, and a broad band from 2400 to 3400 cm^{-1} , corresponding to the OH of the carboxylic acid groups. The halogenation of DFA was confirmed by the disappearance of the OH band around 3000 cm^{-1} , as well as the shift of the carbonyl group band from 1707 to 1798 cm^{-1} due to the formation of more electron withdrawing chloride groups. $^1\text{H-NMR}$ analysis and more particularly the deshielding effect of the methylene group attached to the carboxylic acid (from 2.35 to 2.88 ppm) also confirm the halogenation (Figure 4).

The chemical structures of DBISCC were analyzed and confirmed by FTIR and NMR spectroscopies (Figures 3, 4 and S5 in the ESI⁺):

FTIR-ATR (cm^{-1} , Figure 3): 1740 (C=O ester group), 1797 (C=O cyclocarbonate group).

$^1\text{H-NMR}$ (300 MHz, CDCl_3 , δ , ppm, Figure 4): 0.81-0.90 (6H, m, -CH₃), 1.25 (38H, s, -CH₂-), 1.56-1.66 (4H, m, -CH₂-CH₂-COO-), 2.36 (4H, t, $J = 7.6$ Hz, -CH₂-CH₂-COO-), 4.22-4.39, 4.55 (8H, m, t, $J = 8.6$ Hz, -OCOO-CH₂-CH-CH₂-O-), 4.88-4.96 (2H, m, -OCOO-CH₂-CH-CH₂-O-), 5.00-5.45, 6.69-7.12 (0.82H, m, -CH=CH-).

$^{13}\text{C-NMR}$ (100 MHz, CDCl_3 , δ , ppm, Figure S5 in the ESI⁺): 14.3 (-CH₃), 22.8 (-CH₂-CH₃), 24.9 (-CH₂-CH₂-COO-), 29.1-30.2 (-CH₂-), 34.0 (-CH₂-COO-), 62.9 (-OCOO-CH₂-CH-CH₂-O-), 66.1 (-OCOO-CH₂-CH-CH₂-O-), 73.9 (-OCOO-CH₂-CH-CH₂-O-), 154.5 (-OCOO-), 173.4 (-COO-).

The esterification reaction of DCI with GC results in modification of the carbonyl group region, observed through FTIR analysis. Whereas carbonyl bands related to chloride groups disappear in favor of the ester carbonyl group band at 1740 cm^{-1} , an additional peak at 1797 cm^{-1} confirms the presence of carbonate groups (Figure 3). The esterification reaction was also confirmed by NMR analysis, the results of which are presented in Figure 4. The methylene group linked to the chloride function shifts from 2.88 to 2.36 ppm due to the formation of the ester, a less electronegative group. Furthermore, some peaks assigned to the cyclic carbonate group appear in the region 4.2-5.0 ppm. Carbon double bonds are still present, as shown by their signals at approx. 5.3 and 6.8 ppm.

3.2. DNIPU characterization

3.2.1 Effect of the DBisCC:diamine molar ratio. A first study was performed to determine the optimal ratio for the NIPU synthesis. Figure 5 shows the storage modulus (G') and loss factor ($\tan \delta$) as function of temperature for DNIPU-DDA2.0 based on different DBisCC:diamine molar ratios in a large temperature range from 5 to 130°C. Two different behaviors were observed:

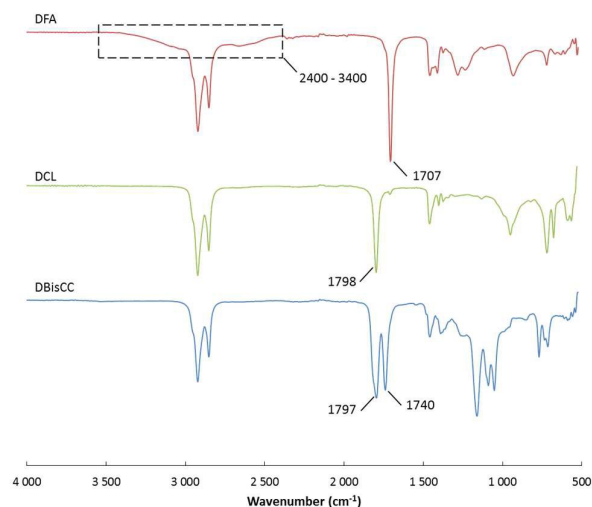


Figure 3. FTIR spectra of intermediates based on DFA.

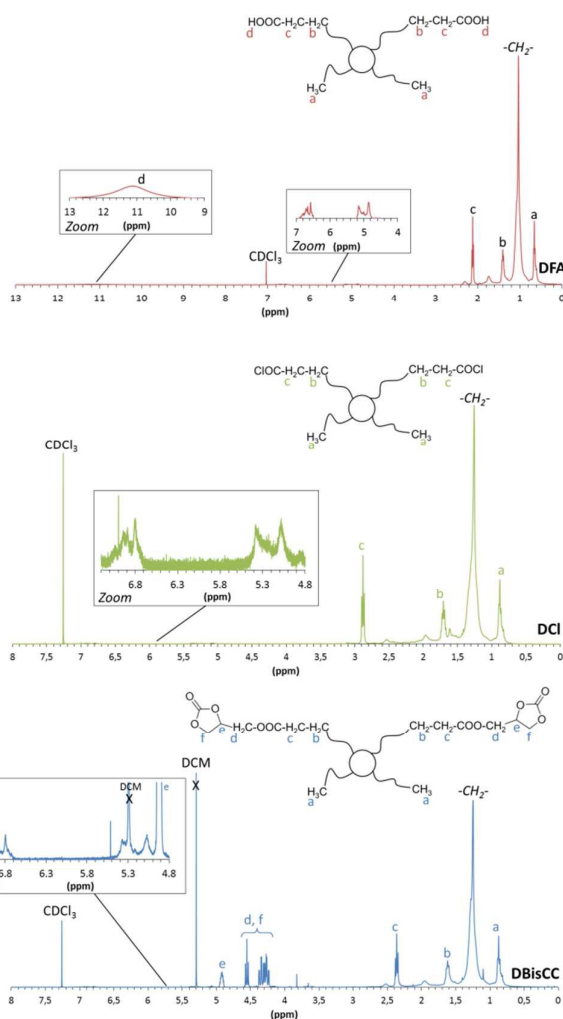


Figure 4. $^1\text{H-NMR}$ spectrum of intermediates based on DFA.

(i) For a stoichiometric ratio: a short rubbery plateau is visible on the storage modulus curve, which shows a particular structuration due to a network formation. The maximum loss factor value, lower than one, corroborates this result.

(ii) For a non-stoichiometric ratio: the G' moduli drop and $\tan \delta$ quickly rises, meaning that the materials flow and do not have a specific structuration. Shorter chains are formed. With an excess of amine, secondary reactions with ester linkages can occur with a decrease of the chain length as mentioned by Javni *et al.*^{32, 33} The resulting amide linkages were confirmed by FTIR analysis (Figure S6 in the ESI[†]) and were already noted for other NIPU materials.²⁹ All things considered, the stoichiometric ratio was selected for the further studies.

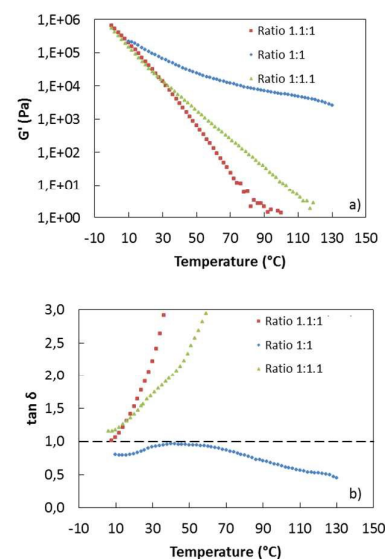


Figure 5. Dynamic rheological analysis curves of DNIPU-fn=2.0 based on various molar ratios.

DNIPU-1.1:1 ratio (■), DNIPU-1:1 ratio (●), DNIPU-1:1.1 ratio (▲).
a) storage modulus, G' ; b) loss factor, $\tan \delta$.

3.2.2. Effect of the average amine functionality. DNIPUs were synthesized from dimeric bis(cyclic carbonates), varying their average amine functionalities from 2.0 to 2.2. They are referred to as DNIPU-DDA2.0, 2.05, 2.1, 2.15 and 2.2, respectively. Chemical characterizations of these materials were performed to define their structures and to analyze the influence of the average amine functionality on their structures and their corresponding thermal and rheological properties.

The characteristic bands of DNIPUs were observed by FTIR analysis (Figure S7 in the ESI[†]). Except for DNIPU-DDA2.05, DNIPU samples are not soluble in common solvents. They are mainly thermoset polymers and form polymeric gels. The results obtained from swelling data of DNIPU samples in tetrahydrofuran are summarized in Table 5. Except DNIPU-DDA2.05, all polymers are crosslinked. However, their gel values are quite low and DNIPUs contain approx. 30% of soluble fractions, compared with a few percent for conventional PUs.³⁴ This difference can be explained by chain cleavages due to secondary reactions between amines and ester links.^{32, 33} High SR values indicate low crosslinking degrees. One can

remark that the SR has a tendency to decrease as the average amine functionality increases.

Table 5. Gel content and degree of swelling of DNIPU thermosets.

Samples	G (%)	SR (%)
DNIPU-DDA2.0	75	2000
DNIPU-DDA2.05	soluble	soluble
DNIPU-DDA2.1	70	1970
DNIPU-DDA2.15	67	1740
DNIPU-DDA2.2	66	1450

Table 6 shows the T_g values of the synthesized DNIPUs. All values of T_g are quite low (around -20°C) compared to those of conventional NIPUs² due to the dimeric structures with pendant aliphatic chains, which increase the free volume and, consequently, the chain mobility. Average amine functionality does not seem to significantly influence the T_g value. DNIPUs have rather low degrees of crosslinking, which can be approximated from the inverse of the SR value (Table 7). Thus, these corresponding variations are too low to have a significant impact on the T_g values.

Table 6. DSC data of DNIPU samples.

Samples	T_g ($^\circ\text{C}$)
DNIPU-DDA2.0	-20
DNIPU-DDA2.05	-21
DNIPU-DDA2.1	-21
DNIPU-DDA2.15	-20
DNIPU-DDA2.2	-19

The thermal degradation of DNIPUs and their monomers was investigated *via* TGA (Figure 6 and Table S1 in the ESI[†]). As with the corresponding dimeric acids and derivatives, all DNIPUs display a global good thermal stability with a maximum degradation between 442 and 452 $^\circ\text{C}$ (Table S1 in the ESI[†]). However, we can notice that the degradation starts at very low temperature (around 200 $^\circ\text{C}$), which could limit the applications for these materials. The degradation windows of the DNIPUs are very large. DDA2.0 shows a well-defined degradation step, whereas DDA2.2 presents a broader transition towards higher temperatures. This is due to the higher trimer content within DDA2.2, forming a crosslinked network and increasing the thermal resistance. The thermal decomposition of conventional PUs is usually a multi-stage process including the decomposition of urethane bonds and the degradation of the corresponding carbonated chains.³⁵ The degradation of the DNIPUs presents different main steps. The large temperature range, till 400 $^\circ\text{C}$, indicates that the first degradation step is a combination of various degradation processes. It could be largely assigned to the decomposition of both urethane and ester linkages.³⁶ The last degradation step (400 to 500 $^\circ\text{C}$), which is more noticeable, could be attributed to the degradation of the carbonated segments. More

details are given below for the comparison of the thermal degradation of PUs and NIPUs.

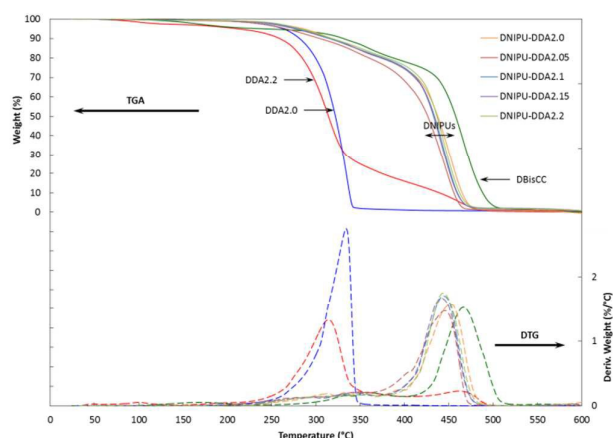


Figure 6. TGA (solid line) and DTG (dotted line) curves of DNIPUs and their monomers under nitrogen.

Table S1 in the ESI[†] demonstrates that the average amine functionality appears to have a small influence on the thermal degradation of DNIPUs. DNIPU-DDA2.05, based on a non-crosslinked structure, is more thermally sensitive. The corresponding degradation begins slightly before those of the other DNIPUs. Considering the $T_{2\%}$ values, higher degradation temperatures are obtained when the average amine functionality increases. This should be due to higher trimer contents in the initial compounds and, therefore, also in the macromolecular architectures. The TGA analysis also confirmed that in the temperature domain explored by DSC, DNIPUs are not degraded. Rheological analyses were performed in order to obtain further information on the morphology of these DNIPUs. Figure 7 shows the dependence on temperature of the storage moduli (G') of the DNIPUs. The curves from Figure 7 indicate that the rheological behavior of the DNIPUs is influenced by the average amine functionality. Except for DNIPU-DDA2.05, whose storage modulus drops with increasing temperature, all the samples present a rubbery plateau at a temperature higher than 80 $^\circ\text{C}$ (Figure 7). This plateau confirms their crosslinked states. Two main behaviors are highlighted, with a transition at an average amine functionality between 2.05 and 2.1. For crosslinked DNIPUs, the rubbery plateau becomes higher and longer with increasing average amine functionality, which confirms the rising trend of the crosslinking density (approximated from the previous SR ratio calculations). It should be noted that DNIPU-DDA2.0 is a particular case and shows a rubbery plateau despite its low average amine functionality. Table 5 shows that the gel content value found for DNIPU-DDA2.0 is the highest among all DNIPU samples. This means that, in this case, secondary reactions are lower and the molar masses are higher compared to the other DNIPU samples with higher average amine functionalities. This could explain the better structuration of DNIPU-DDA2.0.

All these results confirm that tailoring the properties of these DNIPU systems is possible *via* a modulation of the average amine functionality.

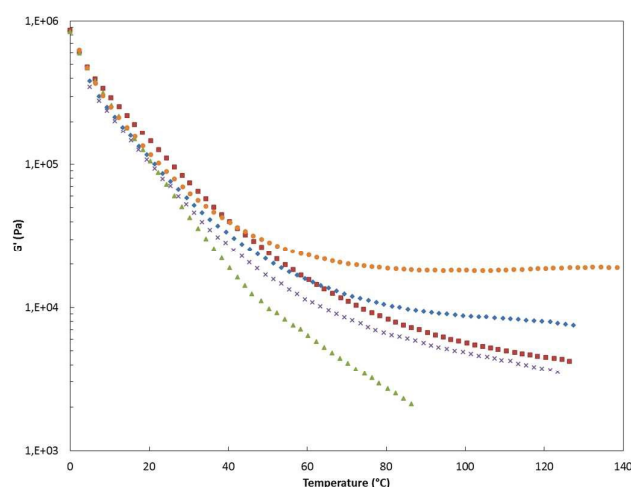


Figure 7. Dynamic rheological curves of DNIPU samples, evolution of storage moduli (G'). DNIPU-DDA2.0 (■), DNIPU-DDA2.05 (▲), DNIPU-DDA2.1 (×), DNIPU-DDA2.15 (◆), and DNIPU-DDA2.2 (●).

3.2.3. Analysis of the mechanical properties of DNIPU-DDA2.0.

Considering DNIPU-DDA2.0, additional tests were performed to determine the mechanical behavior of this particular system. The stress-strain curves of DNIPU-DDA2.0 samples obtained from uniaxial tensile tests are typical of elastomeric behavior with a high elongation at break, $\epsilon_{\max} = 1280 \pm 10\%$ (Figure S8 in the ESI†). This high elongation is explained by a specific structuration, linked to a low crosslink density. However, the ultimate tensile strength, $\sigma_{\max} = 0.5 \pm 0.1$ MPa, is quite low compared to the great majority of common elastomers.²¹ The Young's modulus, $E = 0.20 \pm 0.03$ MPa, was also determined from the stress-strain curves. This low value is typical of very soft elastomers.

3.3. Analysis of the relationships between the chemical structure of the building blocks (dimeric vs. linear) and the properties of the corresponding NIPUs.

To analyze the “chemical structure-properties” relationships, different NIPUs have been synthesized from dimeric or, more conventional, linear building blocks. DNIPU-DDA2.0 and LNIPU-DDA2.0 have been synthesized from dimeric diamine DDA2 with one of two different bis(cyclic carbonate)s, dimeric DBisCC or linear LBisCC, respectively. In addition, DNIPU-DDA2.0 and DNIPU-DA8 have been synthesized from the same dimeric bis(cyclic carbonate) and two different diamines, the dimer DDA2 or the linear DA8, respectively. Analyses have been performed on these two classes of NIPU to investigate the influence of cyclic carbonate and amine structures (dimeric vs. linear structures) on some final material properties.

Figure 8 displays the TGA and DTG curves of DNIPU samples under nitrogen atmosphere. It can be observed that the structures of the cyclic carbonate and amine building blocks strongly affect the thermal degradation.

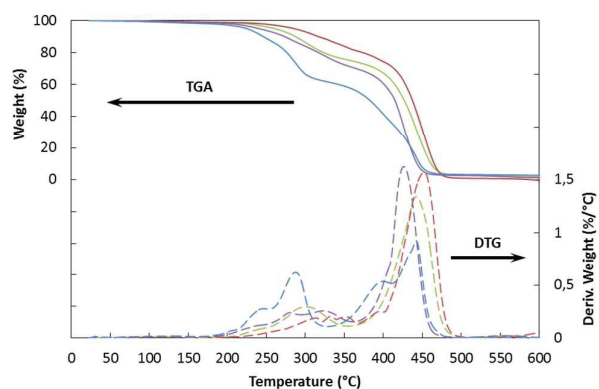


Figure 8. TGA (solid line) and DTG (dotted line) curves of NIPU samples. DNIPU-DDA2.0 (in red), DNIPU-DA8 (in green), LNIPU-DDA2.0 (in purple), and LNIPU-DA8 (in blue).

As can be observed from Table 7, the T_{\max} value of DNIPU-DDA2.0 is 30°C higher than the T_{\max} value of LNIPU-DDA2.0. NIPUs synthesized with DBisCC present a higher thermal stability than those obtained from linear LBisCC. This higher resistance is due to (i) the cyclic structures of DBisCC and (ii) the presence of trimers, which both enhance the thermal degradation. The same effect is also observed for NIPUs obtained with BisCC and a linear or dimeric diamine. For instance, DNIPU-DDA2.0 presents a higher thermal stability with a T_{\max} value about 10°C higher than that of DNIPU-DA8 (Table 7). The difference in thermal stability is, thus, less noticeable for diamine structures compared to cyclic carbonates. This could be explained by the effect of the trimer content, which is higher for DBisCC (about 3%) than for DDA2 (less than 1%), whereas it is quite the same for both linear and dimeric diamines. Furthermore, as the purity of the building blocks decreases, the DTG curve becomes broader with no distinctive peak between 200 and 400°C. This large range is caused by the diversity in the dimeric structures of DDA2 (acyclic, monocyclic, and bicyclic) in addition to the effect of the trimers. Each of these particular structures presents its own degradation temperatures and steps.

Table 7. NIPUs characteristic temperatures obtained from TGA and DSC.

Samples	$T_{98\%}$ (°C)	$T_{50\%}$ (°C)	$T_{2\%}$ (°C)	T_{\max} (°C)	T_g (°C)	T_m (°C)
DNIPU-DDA2.0	245	437	479	452	-20	-
DNIPU-DA8	226	427	573	442	-16	41
LNIPU-DDA2.0	206	415	548	426	-23	-
LNIPU-DA8	178	383	600	442	-17	38

TGA results show that in the temperature range explored by DSC, NIPUs are not degraded (Table 7). As for the case of bis(cyclic carbonate) (previously presented), the amine chemical structure does not significantly affect the T_g values of the NIPUs (Table 7). All NIPUs present a low T_g at around -20°C. However, when DA8 is used as a building block, the T_g is slightly higher due to a decrease of the chain mobility and a melting temperature peak appears. Semi-crystalline polymers are, thus, obtained with linear diamines.

Dynamic rheological analyses display complementary information about the macromolecular architecture of the different NIPUs. Figures 9 and 10 show the influence of the NIPU structure on the storage modulus, as well as on the tangent delta. They highlight two different behaviors, that is, that linear LNIPUs flow as temperature is increased, whereas DNIPUs present a rubbery plateau indicating a certain structuration (Figure 9). This structuration could be due to the presence of a trimer content of 3%, which is enough to induce the crosslinking responsible for the formation of a network. However, as shown before, the crosslinking density is low and the value of the storage modulus on the rubbery plateau is lower than for conventional thermoset polymers.³⁷ As it appears in Figure 10, only DNIPU-DDA2.0 presents an alpha relaxation temperature, determined at a maximum of the tangent delta. The maximum of the tangent delta is lower than 1. The elastic component is always higher than the viscous component. This sample shows the highest structuration.

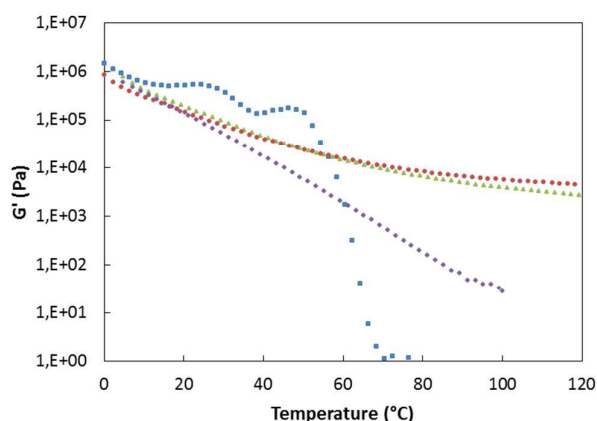


Figure 9. Dynamic rheological analyses of NIPU samples. Influence of the building block structure on the storage modulus. DNIPU-DDA2.0 (●), DNIPU-DA8 (▲), LNIPU-DDA2.0 (◆), and LNIPU-DA8 (■).

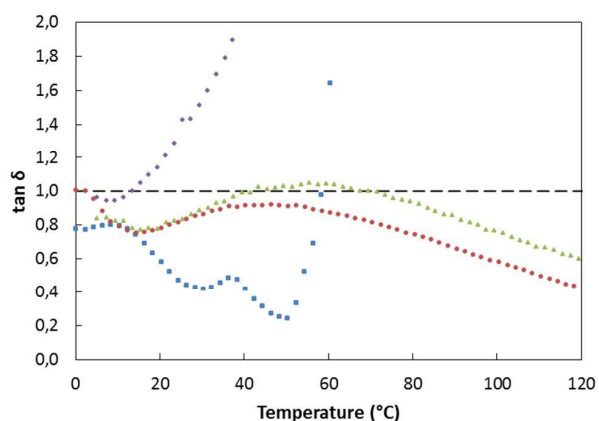


Figure 10. Dynamic rheological analyses of NIPU samples. Influence of the building block structure on the tangent delta. DNIPU-DDA2.0 (●), DNIPU-DA8 (▲), LNIPU-DDA2.0 (◆), and LNIPU-DA8 (■).

3.4. Comparison between NIPUs and conventional PUs based on equivalent structures

Conventional PUs were synthesized with both dimeric and linear polyols and isocyanates to enable a comparison with analogous NIPUs. It should be noted that even with equivalent building blocks, the chemical structures of the NIPUs and PUs differ based on the presence of OH groups (PHU). These OH functions increase the number of hydrogen bonds and, as such, the possibility to cause potential post-reactions.

SEC results are presented in Table 8. As expected, PUs present higher molar masses than NIPUs caused by the limited reactivity of cyclic carbonates towards diamines due to the existence of secondary reactions like ester aminolysis or urea formation.³⁸ Compared to DPUs, DNIPUs are not soluble in common solvents, probably due to the trimer building blocks in the corresponding macromolecular architectures. In addition, the hydrogen bonds linked to the OH groups in NIPUs could also limit the DNIPUs solubility in some common solvents.

Table 8. Results of SEC analysis of NIPUs and PUs.

Samples	M_n ($\text{g}\cdot\text{mol}^{-1}$)	M_w ($\text{g}\cdot\text{mol}^{-1}$)	\bar{D}
DNIPU-DDA2.0	Not soluble in common solvents		
DNIPU-DA8	Not soluble in common solvents		
LNIPU-DDA2.0	6,000	20,000	3.1
DPU-DOH	36,000	89,500	2.5
DPU-OH8	35,000	73,500	2.1
LPU-DOH	17,400	33,000	1.9

Table 9 shows the thermal analysis results of the PUs. T_{max} values indicate that all NIPUs have higher thermal stability than their corresponding PUs (Table 7). As for NIPUs, the fully dimer-based PU presents the highest thermal resistance. This phenomenon highlights again the positive impact of the dimeric structure on the thermal resistance of the corresponding polymers.

Table 9. Characteristic temperatures of PUs from TGA and DSC characterizations.

Samples	$T_{98\%}$ (°C)	$T_{50\%}$ (°C)	$T_{2\%}$ (°C)	T_{max} (°C)	T_g (°C)	T_m (°C)
DPU-DOH	350	422	505	419	-25	-
DPU-OH8	341	398	426	406	-12	55
LPU-DOH	340	413	514	394	-18	63

Except for the DPU-DOH sample, which is a fully amorphous polymer with a low T_g similar to NIPUs, PUs have a 10°C higher T_g than those of NIPUs (Tables 7 and 9). Furthermore, DPU-OH8 and LPU-DOH present a melting temperature and are semi-crystalline structures. The highest molar masses give a better structuration of the samples and linear monomers can play their conventional role in the reorganization of these systems.

Conclusions

A two-step method for the preparation of a dimer-based cyclic carbonate was developed. This cyclic carbonate and its derivatives were then characterized and subsequently used as building blocks for NIPU synthesis. Fully biobased NIPUs, from dimeric cyclic carbonate and dimeric diamines were synthesized and characterized. The importance of a stoichiometric ratio and the influence of the average amine functionality were highlighted. Upon increasing the average amine functionality, a crosslinked network is formed. NIPUs with various macromolecular architectures were also designed and the effect of the chemical structure of the building block on their thermal, rheological and mechanical properties was investigated. It was shown that the dimeric structure affects the properties of the NIPU and particularly increases the thermal stability of the corresponding polymers. But the key factor linked to the properties of these polymers is the dimer composition. A small percentage of trimers in the bicyclic carbonate or diamine seems to increase the crosslinking density and bring some specific structuration. However, even if NIPUs display promising properties, their values are consistently lower than those of conventional PUs based on equivalent dimeric structures. The main reason for such differences is the low reactivity of the aminolysis reaction compared to conventional reactions based on isocyanates. Thus, lower molar masses were obtained for NIPUs compared to PUs. Nevertheless, it was demonstrated that NIPUs based on crosslinks to prepare specific networks can partially fill in these gaps.

Acknowledgements

The authors thank the Alsace Region, the urban community of Strasbourg, SOPREMA and PSA Peugeot Citroën for their financial supports. Cognis-BASF, Croda, Huntsman, Oléon and Vencorex are also acknowledged for having kindly provided raw materials, and NMRTec for having performed the DOSY NMR analyses. The authors are grateful to Prof. Jean-Pierre Pascault (IMP-INSA Lyon, France), Dr. Sylvain Caillol (ENSCM), Dr. Sébastien Gallet (ICPEES Strasbourg, France) for helpful discussions and to Dr. Zarah Walsh-Korb for the English corrections.

References

- D. P. Pfister, Y. Xia and R. C. Larock, *ChemSusChem*, 2011, **4**, 703.
- B. Nohra, L. Candy, J.-F. Blanco, C. Guerin, Y. Raoul and Z. Mouloungui, *Macromolecules*, 2013, **46**, 3771.
- C. Bueno-Ferrer, E. Hablot, M. Del Carmen Garrigos, S. Bocchini, L. Averous and A. Jiménez, *Polym. Degrad. Stab.*, 2012, **97**, 1964.
- C. Bueno-Ferrer, E. Hablot, F. Perrin-Sarazin, M. C. Garrigós, A. Jiménez and L. Averous, *Macromol. Mater. Eng.*, 2012, **297**, 777.
- A. S. More, T. Lebarbé, L. Maisonneuve, B. Gadenne, C. Alfes and H. Cramail, *Eur. Polym. J.*, 2013, **49**, 823.
- G. Çaylı and S. Küsefoğlu, *J. Appl. Polym. Sci.*, 2008, **109**, 2948.
- L. Hojabri, X. Kong and S. S. Narine, *Biomacromolecules*, 2009, **10**, 884.
- L. Hojabri, X. Kong and S. S. Narine, *J. Polym. Sci., Part A: Polym. Chem.*, 2010, **48**, 3302.
- M. Charlon, B. Heinrich, Y. Matter, E. Couzigné, B. Donnio and L. Avérous, *Eur. Polym. J.*, 2014, **61**, 197.
- X. Baur, W. Marek, J. Ammon, A. B. Czuppon, B. Marczyński, M. Raulf-Heimsoth, H. Roemmelt and G. Fruhmann, *Int. Arch. Occup. Environ. Health*, 1994, **66**, 141.
- M. S. Kathalewar, P. B. Joshi, A. S. Sabnis and V. C. Malshe, *RSC Adv.*, 2013, **3**, 4110.
- J. Guan, Y. H. Song, Y. Lin, X. Z. Yin, M. Zuo, Y. H. Zhao, X. L. Tao and Q. Zheng, *Ind. Eng. Chem. Res.*, 2011, **50**, 6517.
- H. Tomita, F. Sanda and T. Endo, *J. Polym. Sci., Part A: Polym. Chem.*, 2001, **39**, 851.
- S. Benyahya, M. Desroches, R. Auvergne, S. Carlotti, S. Caillol and B. Boutevin, *Polym. Chem.*, 2011, **2**, 2661.
- M. O. Sonnati, S. Amigoni, E. P. Taffin de Givenchy, T. Darmanin, O. Choulet and F. Guittard, *Green Chem.*, 2013, **15**, 283.
- H. Baumann, M. Bühler, H. Fochem, F. Hirsinger, H. Zobebelein and J. Falbe, *Angew. Chem., Int. Ed. Engl.*, 1988, **27**, 41.
- A. Vasishta, R. Trivedi and G. Das, *J. Am. Oil Chem. Soc.*, 1990, **67**, 333.
- C. Jiménez-Rodríguez, G. R. Eastham and D. J. Cole-Hamilton, *Inorg. Chem. Commun.*, 2005, **8**, 878.
- H. Ngo and T. Foglia, *J. Am. Oil Chem. Soc.*, 2007, **84**, 777.
- S. Huf, S. Krügener, T. Hirth, S. Rupp and S. Zibek, *Eur. J. Lipid Sci. Technol.*, 2011, **113**, 548.
- H. Panda, *Handbook on Oleoresin and Pine Chemicals (Rosin, Terpene Derivatives, Tall Oil, Resin & Dimer Acids)*, NIIR Project Consultancy Services, 2008.
- H. Tomita, F. Sanda and T. Endo, *J. Polym. Sci., Part A: Polym. Chem.*, 2001, **39**, 162.
- H. Tomita, F. Sanda and T. Endo, *J. Polym. Sci., Part A: Polym. Chem.*, 2001, **39**, 860.
- C. D. Diakoumakos and D. L. Kotzev, *Macromol. Symp.*, 2004, **216**, 37.
- F. Camara, S. Benyahya, V. Besse, G. Boutevin, R. Auvergne, B. Boutevin and S. Caillol, *Eur. Polym. J.*, 2014, **55**, 17.
- M. Blain, L. Jean-Gérard, R. Auvergne, D. Benazet, S. Caillol and B. Andrioletti, *Green Chem.*, 2014, **16**, 4286.
- H. Tomita, F. Sanda and T. Endo, *J. Polym. Sci., Part A: Polym. Chem.*, 2001, **39**, 3678.
- L. Maisonneuve, A. L. Wirotius, C. Alfes, E. Grau and H. Cramail, *Polym. Chem.*, 2014, **5**, 6142.
- C. Carré, L. Bonnet and L. Averous, *RSC Adv.*, 2014, **4**, 54018.
- A. Jerschow and N. Müller, *J. Magn. Reson.*, 1997, **125**, 372.
- K. F. Morris and C. S. Johnson, *J. Am. Chem. Soc.*, 1992, **114**, 3139.
- I. Javni, D. P. Hong and Z. S. Petrovic, *J. Appl. Polym. Sci.*, 2008, **108**, 3867.
- I. Javni, D. P. Hong and Z. S. Petrović, *J. Appl. Polym. Sci.*, 2013, **128**, 566.
- E. Hablot, D. Zheng, M. Bouquey and L. Avérous, *Macromol. Mater. Eng.*, 2008, **293**, 922.
- J. H. Saunders, *Rubber Chem. Technol.*, 1959, **32**, 337.
- S. Yadav, F. Zafar, A. Hasnat and S. Ahmad, *Prog. Org. Coat.*, 2009, **64**, 27.
- J. P. Pascault and R. J. J. Williams, in *Thermosets: Structure, Properties And Applications*, ed. Q. Guo, Woodhead Publishing Ltd., 2012, ch. 1, pp. 3-27.
- V. Besse, F. Camara, F. Méchin, E. Fleury, S. Caillol, J.P. Pascault and B. Boutevin, *Eur. Polym. J.*, **71**, 1.

Graphical Abstract

Solvent- and catalyst-free synthesis of fully biobased nonisocyanate polyurethanes with different macromolecular architectures.

C. Carré,^a L. Bonnet^a and L. Avérous^a

